Statistics of Fluctuating Colloidal Fluid-Fluid Interfaces

V.W.A. de Villeneuve[1], J.M.J. van Leeuwen[2],
W. van Saarloos[2] and H.N.W. Lekkerkerker[1].

[1] Van 't Hoff Laboratory for Physical and Colloid Chemistry,
University of Utrecht, Padualaan 8, 3584 CH Utrecht, The Netherlands
[2] Instituut-Lorentz, Leiden University, Niels Bohrweg 2,
Leiden, 2333 CA, The Netherlands

June 18, 2008

PACS **05.40.-a** –Fluctuation phenomena, random processes,
noise and Brownian motion
PACS **68.03.Kn** –Fluid interfaces
PACS **82.70.Dd** –Colloids
PACS **87.64.Tt** –Confocal Microscopy

Abstract

Fluctuations of the interface between coexisting colloidal fluid phases have been measured with confocal microscopy. Due to a very low surface tension, the thermal motions of the interface are so slow, that a record can be made of the positions of the interface. The theory of the interfacial height fluctuations is developed. For a host of correlation functions, the experimental data are compared with the theoretical expressions. The agreement between theory and experiment is remarkably good.

1 Introduction

The study of interfaces has a long and interesting history. In 1894 van der Waals [1] proposed an interface theory, which leads to a flat interface with a density profile in the direction of gravity. This result is sometimes referred to as the *intrinsic interface*. Already von Schmoluchowski [2] realized that the thermal motion of the molecules induces height fluctuations in the interface. These motions have been called *capillary waves*, since they derive from an interplay of gravity and surface tension, like capillary rise. The fluctuations were first treated theoretically and experimentally by Mandelstam [3]. He pointed out that the interface width diverges due to the short wavelength capillary waves. This fact was rediscovered by Buff, Lovett and Stillinger [4] fifty years later, after which it obtained a prominent place in the discussion of interfaces. Weeks [5] later pointed out that the notion of capillary waves only applies to wave lengths larger than the fluid correlation length, which is of the order of the interparticle distance.

The experimental study of interfaces was undertaken by Raman [6] and Vrij [7] with light scattering and starting with Braslau et al. [8] by X-ray scattering. Although

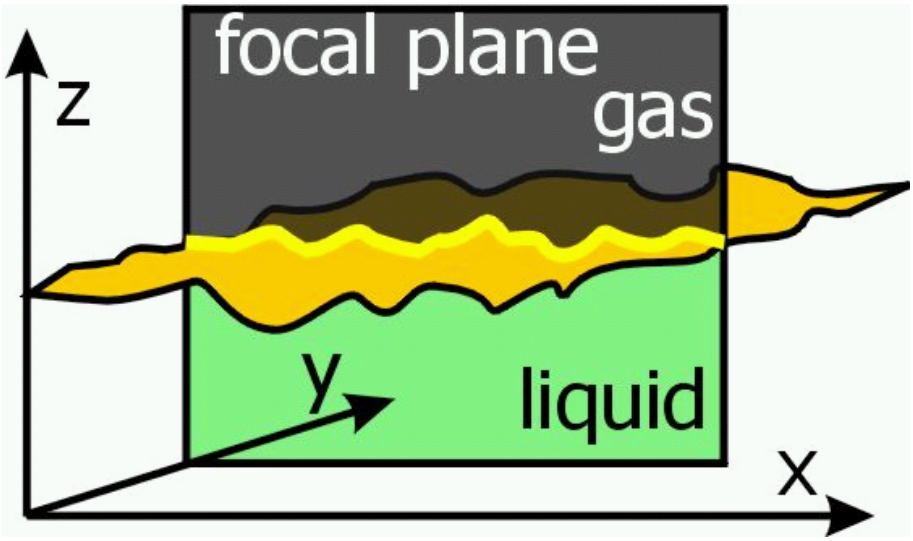

Figure 1: Schematic view of Confocal Microscopy. The confocal microscope thin focal planes of approximately 500 nm thickness can be imaged. This enables the investigation of local phenomena such as height fluctuations.

scattering on interfaces is most valuable, it always yields *global* information on the fluctuations, while a photographic inspection gives *local* information. However, the wave lengths and heights involved in the capillary waves of molecular fluids are way out of the reach of detection by photographic methods. The visual inspection of capillary waves initially remained restricted to computer simulations of interfaces in molecular systems [9].

The field obtained another dimension by recent experiments of Aarts et al. [10] in which they obtained pictures of fluctuating colloidal interfaces. The key is that, by lowering the surface tension to the nN/m range, the characteristic length and time scale of the fluctuations become accessible by confocal microscopy. This opened up the possibility to follow in detail the motion of the height of the interface and to do a statistical analysis of its temporal and spatial behavior. Of course the method has its inherent restrictions. Just as in ordinary movie recording, the pixels have a finite distance and the snapshots have to be taken at finite time intervals. For colloidal interfaces this interval can be made much smaller than the intrinsic time scale of the motions. Thus the Brownian character of the motion could be demonstrated *ad oculos*.

In the confocal microscopy a two-dimensional section is inspected perpendicular to the interface and the density profile between the two phases is observed. A schematic picture of the experiment is shown in Fig. 1. A very precise location of the interface can be obtained by fitting the intensity with a van der Waals-like profile: $I(z,x) = a + b\tanh([z-h(x)]/c)$, where z is the direction perpendicular to the interface and x a coordinate along the interface. In the upper phase the density approaches a value corresponding to $a+b$ and in the lower phase to $a-b$, while c measures the intrinsic width of the interface. Thus at every snapshot a function $h(x)$ follows and the sequence of snapshots gives the function $h(x,t)$. This is a practical separation of the particle motions, which lead at short scales to the *intrinsic interface* and the particle motions which drive the long wavelength *capillary waves*. One might think that, if the time interval of the snapshots is sufficiently small with respect to the characteristic time scale of variation in $h(x,t)$, one can analyze $h(x,t)$ as a continuous function of the time, like a movie gives the impression of a continuous motions, while it is a succession

of snapshots. In a previous short report [13] on these experiments we have pointed out that the statistics remains dependent on the time interval, due to the Brownian character of the motion.

We have performed confocal microscopy measurements on phase separated colloid-polymer mixtures. The colloids are 69 nm radius fluorescently-labeled polymethylmetacrylate particles, suspended in cis/trans decalin, with polystyrene (estimated radius of gyration = 42 nm [11]) added as depletant polymer. Due to a depletion induced attraction these mixtures phase separate at sufficiently high colloid and polymer volume fractions and a proper colloid to polymer aspect ratio into a colloid-rich/polymer-poor (colloidal liquid) and a colloid-poor/polymer-rich (colloidal gas) phase [12]. Here the polymer concentration acts as an inverse temperature. By diluting several phase separating samples with its solvent decalin, the phase diagram was constructed. With a Nikon E400 microscope equipped with a Nikon C1 confocal scanhead, series of 10 000 snapshots of the interface were recorded at constant intervals Δt of 0.45 s and 0.50 s of two statepoints to be denoted as II and IV. The pixels are separated by a distance $\Delta x = 156nm$ and a single scan takes approximately 0.25 s to complete.

The set-up of the paper is as follows. We start out by discussing the spatial behavior of the data of a single time frame, which requires only equilibrium statistics. The correlation functions and the statistics of hills and valleys in the interface are determined and compared to the theory.

Then we identify the set of interface modes via the fourier decomposition

$$h(\mathbf{x}, t) = \sum_{\mathbf{k}} h_{\mathbf{k}}(t) \exp(i\mathbf{k} \cdot \mathbf{x}). \tag{1}$$

The modes are overdamped in the relevant regime and follow from the macroscopic interface-dynamics. The motion obeys not only the macroscopic equations but is also influenced by noise. We introduce thermal noise through the Langevin equation and calculate the essential height-height correlation function $\langle h(\mathbf{0}, 0)h(\mathbf{x}, t)\rangle$. Via the equivalent Fokker-Planck equation the probabilities on sequences ("histories") of snapshots are determined. The analysis of the distributions of "hills" and "valleys" in the time domain with respect to a level h is similar to the spatial behavior. A special concern is the dependence of the residence time and the waiting time on the used time-interval.

The paper closes with a discussion of the main results.

2 Equal time Correlations

The function $h(\mathbf{x}, t)$ provides a mathematical division between the two coexisting phases which form the interface. The interface is of the solid-on-solid type since so-called overhangs, well-known in lattice theory, are excluded by construction, as to every value of the horizontal coordinate $\mathbf{x}$ and time t one unique height $h(\mathbf{x}, t)$ is associated. The basic function is the height-height correlation function. Due to translational invariance the modes $\mathbf{k}$ are independent and thus the correlation function in space has the fourier decomposition

$$\langle h(\mathbf{0}, 0)h(\mathbf{x}, 0)\rangle = \sum_{\mathbf{k}} \langle |h_{\mathbf{k}}^2|\rangle \exp(i\mathbf{k} \cdot \mathbf{x}) \tag{2}$$

The brackets denote equilibrium averages and $h_{\mathbf{k}}$ is the amplitude of the $\mathbf{k}$-th mode. The distribution of the $h_{\mathbf{k}}$ follows from the Boltzmann factor involving the energy of a

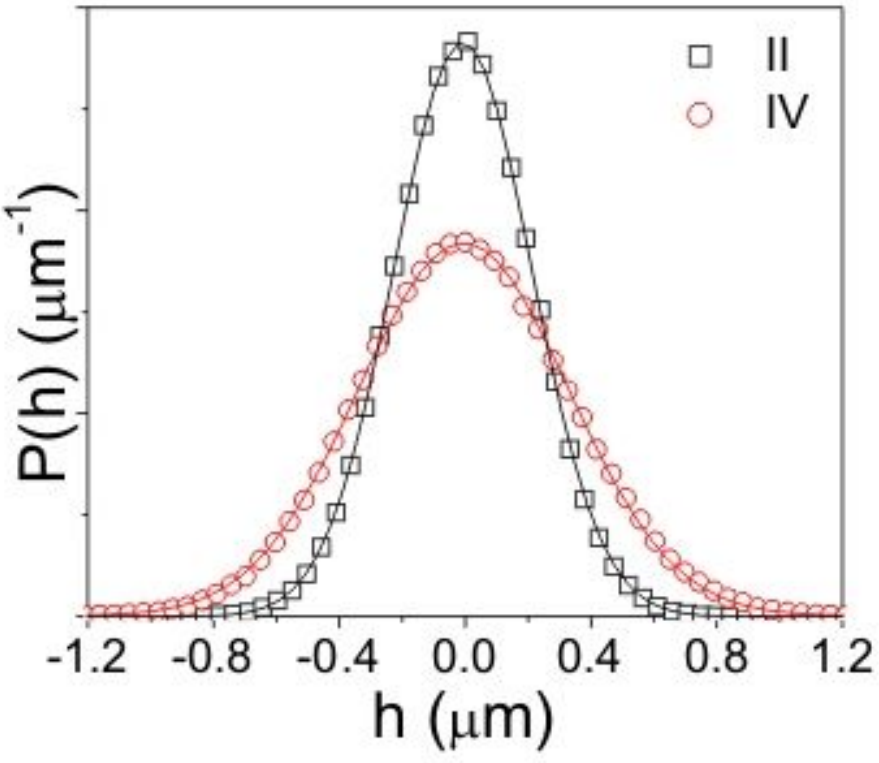

Figure 2: The height distribution for statepoint II and IV as found experimentally. The lines are gaussian fits to the data.

deformation of the interface, which is given by the drumhead model

$$\mathcal{H}(\{h\}) = \frac{1}{2}\int d\mathbf{x}\left[\Delta\rho g h^2(\mathbf{x}) + \gamma(\nabla h(\mathbf{x}))^2\right]. \tag{3}$$

Here $\Delta\rho$ is the density difference between the coexisting phases, γ is the surface tension and g is the gravitational acceleration. The first term gives the gravitational potential energy and the second term the increase of the interfacial energy due to curvature. Expressed in terms of the amplitudes $h_{\mathbf{k}}$ it reads

$$\mathcal{H}(\{h\}) = \frac{L^2}{2}\sum_{\mathbf{k}}[\Delta\rho g + \gamma k^2]\,|h_{\mathbf{k}}|^2, \tag{4}$$

where L^2 is the area of the interface. Since (4) is quadratic in the amplitudes $h_{\mathbf{k}}$, it implies a gaussian distribution for the $h_{\mathbf{k}}$

$$P_e(h_{\mathbf{k}}) = \frac{\exp -|h_{\mathbf{k}}|^2/2\langle|h_{\mathbf{k}}|^2\rangle}{[2\pi\langle|h_{\mathbf{k}}|^2\rangle]^{1/2}}, \tag{5}$$

with the average

$$\langle|h_{\mathbf{k}}|^2\rangle = \frac{k_B T}{L^2(\Delta\rho g + \gamma k^2)}. \tag{6}$$

With the distribution (5) of the $h_{\mathbf{k}}$, we can calculate the distribution of the heights h, which becomes also a gaussian

$$P_{eq}(h) = \frac{\exp(-h^2/2\langle h^2\rangle)}{[2\pi\langle h^2\rangle]^{1/2}}, \tag{7}$$

with the mean square height $\langle h^2 \rangle$ given by

$$\langle h^2 \rangle = \sum_{\mathbf{k}} \langle h_{\mathbf{k}}^2 \rangle = \frac{k_B T}{4\pi\gamma} \ln \frac{1 + k_{max}^2 \xi^2}{1 + k_{min}^2 \xi^2}. \tag{8}$$

ξ is the capillary length defined as

$$\xi^2 = \frac{\gamma}{g\Delta\rho}. \tag{9}$$

The integral has been given an upper bound $k_{max} \simeq 2\pi/d$ with d the diameter of the particles and a lower bound $k_{min} \simeq 2\pi/L$ due to the finite size of the interface. The lower bound can be set equal to 0 for all practical purposes, but the upper bound is essential for the convergence of the integral. Cutting off the capillary waves at the short-wavelength side is the poor man's way to handle the otherwise diverging interface width $\langle h^2 \rangle$. There are two options to determine $\langle h^2 \rangle$. The first follows from a fit to $P_{eq}(h)$, which is shown in Fig. 2. The second is a direct evaluation of $\langle h^2 \rangle$ from the recorded data. The latter always gives a 1-3 % larger value, which we attribute to optical artifacts due to confocal slicing. So we are inclined to prefer the former value which amounts to $\langle h^2 \rangle = 0.219$ for statepoint II and 0.336 $(\mu m)^2$ for statepoint IV. Then equation (8) can be used to estimate the upper cut-off. On the basis of a determination of γ (see below) one finds values around $\kappa = k_{max}\xi \simeq 45$, but this value is rather sensitive to small variations in γ: a variation of γ by 10-15% results in a shift in κ by a factor 2.

The correlation function $\langle h(\mathbf{0}, 0) h(\mathbf{x}, 0) \rangle$ is of course also measurable. In the appendix we discuss the integral (2); here we give the result with the cut-off sent to ∞

$$\langle h(\mathbf{0}, 0) h(\mathbf{x}, 0) \rangle = \frac{k_B T}{2\pi\gamma} K_0(x/\xi). \tag{10}$$

The divergence for $x \to 0$ of the modified Bessel function K_0 corresponds to the divergence of the interface width without a cut-off. A fit of the correlation function to the Besselfunction (with a slight modification due to the cut-off) is shown in Fig. 3. Apart from a few initial points the function fits quite well. We find fitting parameters $\xi = 8.0\mu m$ for statepoint II and $\xi = 6.1\mu m$ for statepoint IV. The values for γ turn out to be $58nN/m$ viz $21nN/m$ for statepoint II viz. IV.

Fourier transforming the correlation function back to the wavenumber domain should lead to the expression (6) as function of k. However, an inverse fourier transform requires accurate data for a large domain and the correlation function is unreliable for large distances (not shown in Fig. 3). This prevents a direct check of the drumhead hamiltonian.

3 Multiple Correlation Functions

As the data are stored for all sampled positions we can determine the probability density

$$G_n(h_1, \mathbf{x}_1; \cdots; h_n, \mathbf{x}_n) = \langle \delta(h(\mathbf{x}_1, 0) - h_1) \cdots \delta(h(\mathbf{x}_n, 0) - h_n) \rangle, \tag{11}$$

which gives the joint probability that the interface at position $\mathbf{x}_1$ has the height h_1 and subsequently at position $\mathbf{x}_i$ the height h_i etc.. A straightforward evaluation of (11)

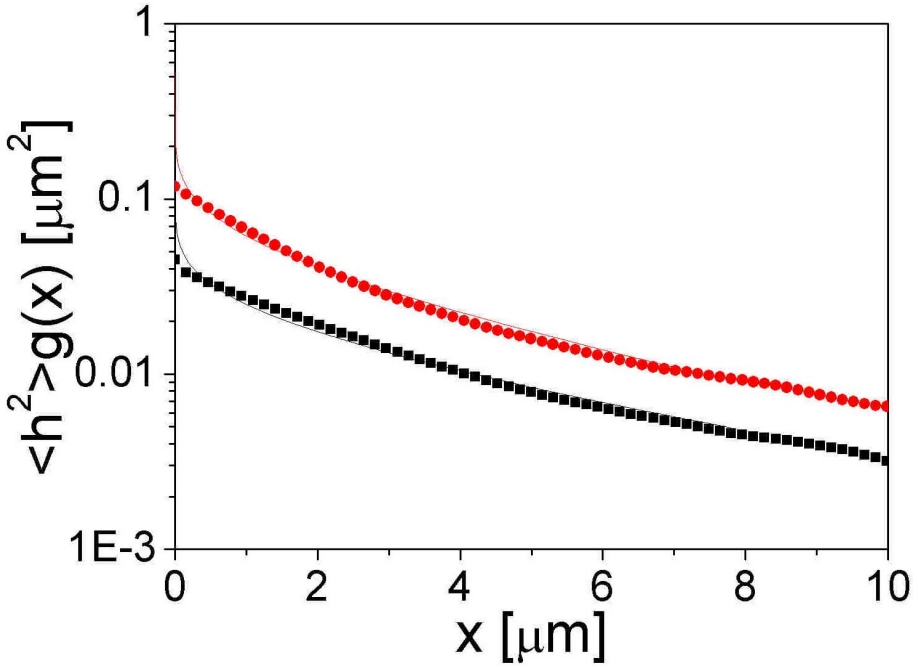

Figure 3: The spatial correlation function $\langle h(x,0)h(0,0\rangle$ for the statepoints II and IV fitted to the expression (10) using a cut-off. The lines are fits to the experimental data.

proceeds via writing the δ functions as a fourier integral and then expressing $h(\mathbf{x},0)$ in terms of the amplitudes $h_{\mathbf{k}}$. As all integrals are over a quadratic form in the exponent the result is a gaussian in the h_i. So one gets an the expression of the type

$$G_n(h_1,\mathbf{x}_1;\cdots;h_n,\mathbf{x}_n) = \left(\frac{\det g^{-1}}{(2\pi\langle h^2\rangle)^n}\right)^{1/2} \exp\left[-\frac{1}{2}\sum_{i,j} g^{-1}_{i,j}\frac{h_i h_j}{\langle h^2\rangle}\right]. \quad (12)$$

In this notation the matrix $g_{i,j}$ is the correlation matrix

$$g_{i,j} = g(|\mathbf{x}_i - \mathbf{x}_j|, 0), \quad (13)$$

which turns out to be the equal-time height-height correlation function

$$g(|\mathbf{x}-\mathbf{x}'|, t-t') = \langle h(\mathbf{x},t)h(\mathbf{x}',t')\rangle / \langle h^2\rangle. \quad (14)$$

A shortcut to the result (12) is to evaluate the following integral in two ways

$$\int dh_1\cdots dh_n\, h_i h_j\, G(h_1,\mathbf{x}_1;\cdots;h_n,\mathbf{x}_n) = \langle h^2\rangle g_{i,j}. \quad (15)$$

The first uses the definition (11) and obviously leads to the right hand side of (15). The second way uses the expression (12). Then one has to diagonalize the quadratic form in the exponent and the integration over the eigendirections also leads to the right hand side of (12), which shows that (13) is correct.

In (14) and accordingly in the result (12), we have factored out $\langle h^2 \rangle$ because we want to use it as a scale for the heights. (12) shows that the correlation function g dictates the behavior of the multiple correlation functions.

To give an impression on the behavior of the G's we first consider a few small values of n. For a single position ($n = 1$) the value $g(0, 0) = 1$ and (12) reduces to the equilibrium height distribution (5)

$$G_1(h_1) = P_{eq}(h_1), \tag{16}$$

which is shown in Fig. 2. From this probability we derive the important probabilities $q^+(h)$ to find a height above h and $q^-(h)$ for finding a height below h. They are given by the expressions

$$q^+(h) = \int_h^\infty P_{eq}(h_1) dh_1, \qquad q^-(h) = \int_{-\infty}^h P_{eq}(h_1) dh_1. \tag{17}$$

In integrals like (17), one changes of course to the combination $h_1/\langle h^2 \rangle^{1/2}$ as integration variable, such that the $q^{\pm}(h)$ become functions of the scaled variable $h/\langle h^2 \rangle^{1/2}$. The result of the integration in (17) is an error function in this parameter. From now on we work with these reduced heights.

The probability density G for $n = 2$ is still sufficiently simple to make it explicit. The matrix $g_{i,j}$ and its inverse $g_{i,j}^{-1}$ read

$$g_{i,j} = \begin{pmatrix} 1 & g_{1,2} \\ g_{2,1} & 1 \end{pmatrix}, \tag{18}$$

and

$$g_{i,j}^{-1} = \frac{1}{1 - g_{1,2}^2} \begin{pmatrix} 1 & -g_{1,2} \\ -g_{2,1} & 1 \end{pmatrix}. \tag{19}$$

So G_2 follows from the general definition as

$$G_2(h_1, \mathbf{0}; h_2, \mathbf{x}) = \frac{1}{2\pi[1 - g^2]^{1/2}} \exp \left[-\frac{h_1^2 - 2gh_1h_2 + h_2^2}{2[1 - g^2]} \right], \tag{20}$$

with g a shorthand for $g_{1,2} = g(x, 0)$ and x the distance of sampling. Note that this expression is symmetric in the entries h_1 and h_2 and that dependence only enters through $g = g(x, 0)$.

4 Statistics of Sequences

The probability densities (11) are measurable, but the statistics becomes poor when too much entries are taken. Therefore integrated probabilities are more accessible. For what follows it is interesting to study the probability that a sequence in space of

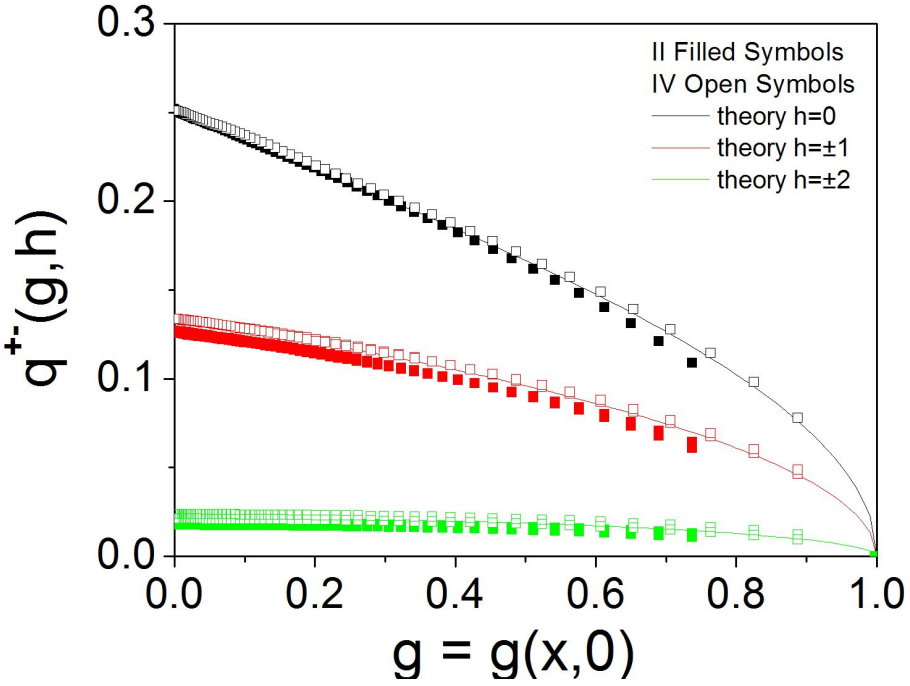

Figure 4: The function $q^{+-}(h,g)$ as function of x through $g = g(x,0)$, for some values of h (in units $\langle h^2\rangle^{1/2}$). The drawn lines are calculated and the points are the measured values.

precisely n successive values occurs of the heights *above* the level h. According to the theory it is given by the ratio of two integrals

$$p_n^+(-h) = q^{-(n+)-}(h)/q^{+-}(h). \tag{21}$$

In this notation the superscript prescribes the integration domain. The numerator of (21) reads

$$q^{-(n+)-}(h) = \int_{-\infty}^{h} dh_0 \int_h^{\infty} dh_1 \cdots \int_h^{\infty} dh_n \int_{-\infty}^{h} dh_{n+1} G_{n+2}(h_0, \cdots, h_{n+1}). \tag{22}$$

The integral over the first variable h_0 guarantees that the sequence starts below level h, the next n integrations select points above the level h and the sequence ends with h_{n+1} below level h. So the numerator in (21) selects the hills of precisely n consecutive values of the height above level h. We have omitted in G_{n+2} the position arguments since it is understood that points are equidistant. So the sequence of values $g(m\Delta x, 0)$ enters, with $0 \le m < n+2$. The denominator is the integral

$$q^{+-}(h) = \int_h^{\infty} dh_1 \int_{-\infty}^{h} dh_2 G_2(h_1, h_2). \tag{23}$$

It counts the number of hills since each hill is followed by a transition from above to below the level h. The denominator serves as a normalizing factor. Summing (21) over n (from 1 to ∞) gives the total number of hills above h and as this equals the number of crossings, we see that the distribution (21) is normalized.

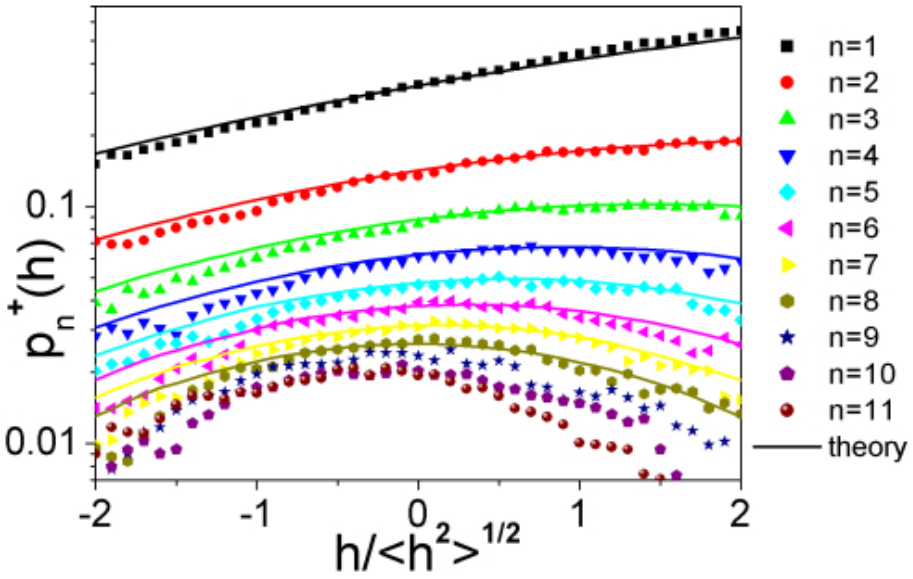

Figure 5: The spatial $p_n^+(h)$ as function of h for a number of n for statepoint IV. The drawn lines are the theoretical values.

The average length $\chi^+(h)$ of a sequence is defined as

$$\chi^+(h) = \sum_{n=1} n p_n^+(h). \tag{24}$$

We also look to sequences *below* the height h. They are given by the probability $p_n^-(h)$ which follows from a similar definition as (21), with + and − interchanged. The up-down symmetry of the problem yields the relation

$$p_n^-(h) = p_n^+(-h). \tag{25}$$

The average length $\chi^-(h)$ of a stretch below h similarly equals

$$\chi^-(h) = \sum_{n=1} n p_n^-(h). \tag{26}$$

Inserting the expression (21) into the definition (24) for $\chi^+(h)$, the numerator in (22) is multiplied by the number of values larger than h. Summation over all n leads to the average number of points above the level h, which is given by the integral (17). Thus we arrive at the relations

$$\chi^\pm(h) = q^\pm(h)/q^{+-}(h). \tag{27}$$

The remarkable point about these relations is that, although the probabilities $p_n^\pm(h)$ are given by multiple integrals, the averages $\chi^\pm(h)$ result from simple integrals. The $q^\pm(h)$ are errorfunctions and q^{+-} is a two-fold integral involving the function G_2, thus containing only the value $g(\Delta x, 0)$.

A trivial result from (27) is that the ratio $\chi^+(h)/\chi^-(h)$ is the same as the ratio $q^+(h)/q^-(h)$. Both give the ratio of the total number of points above and below the level h. As the $q^+(h)$ and $q^-(h)$ add up to 1, a more intriguing result follows for the sum

$$\chi^+(h) + \chi^-(h) = \frac{1}{q^{+-}(h,g)}. \tag{28}$$

Deliberately we have given q^{+-} also the argument g which incorporates the spatial dependence on x. Tacitly we have assumed that this distance is the sampling distance Δx. But nothing prevents us from taking a multiple n of Δx. Then g will refer to $g(n\Delta x, 0)$. In Fig. 4 we have plotted the experimental values of $q^{+-}(h, g)$ for various values of $g(n\Delta x, 0)$, which we take as parameter on the horizontal axis. The curves are the calculated values of $q^{+-}(h, g)$. We have not found a closed expression for q^{+-} in terms of known functions, but a number of limits are explicitly obtainable. The g dependence is exemplified by the case $h = 0$, which reads

$$q^{+-}(0, g) = \frac{1}{2} - \frac{1}{\pi} \arctan \left(\frac{1+g}{1-g} \right)^{1/2}. \tag{29}$$

The h dependence is by and large controlled by the limiting behavior

$$q^{+-}(h, 0) = q^{+}(h) q^{-}(h),$$

$$q^{+-}(h, g \to 1) \simeq \frac{\sqrt{1-g}}{\pi\sqrt{2}} \exp\left[-\frac{h^2}{2\langle h^2 \rangle} \right]. \tag{30}$$

Apart from the averages also the individual $p_n^{\pm}(h)$ can be measured and compared with the theoretical expressions (21). In Fig. 5 we show $p_n^{+}(h)$ for statepoint IV as a function of h for a number of n. The theory requires the evaluation of multiple integrals (22) which can be carried out by Monte-Carlo integration. The best procedure is to generate a distribution according to the gaussian integrand and then reject the points that fall outside the integration domain. This technique also applies to correlation functions for other histories with another integration domain.

The comparison with the theory has been carried out for n up to 8. For higher values of n the integration becomes a bit lengthy for good statistics. The agreement between theory and experiment is good, but typically there are deviations for larger negative values of h, where the experimental points are systematically lower than the theorical prediction.

5 The Dynamic Interface Modes

As the preceding sections show, the interface fluctuations have a rich spatial structure. So it is an interesting question how this compares with the interface fluctuations in time. The temporal development of the interface is determined by the macroscopic equations for the interface modes as well as by the influence of thermal noise. In this section we briefly discuss the interface modes and in the next section we treat the noise.

The problem of the interface modes modes has been addressed by Jeng et al. [14], who have made an extensive study of the interface modes in the various regimes distinguished by the relative strength of viscosity and surface tension. The modes are overdamped for our experimental conditions and decay as

$$h_{\mathbf{k}}(t) = h_{\mathbf{k}} \exp(-\omega_k t), \tag{31}$$

with a rate

$$\omega_k = \frac{1}{2t_c}[(k\xi)^{-1} + k\xi], \tag{32}$$

where the capillary time t_c is given by

$$t_c = \frac{(\eta + \eta')}{\sqrt{g\gamma\Delta\rho}}. \tag{33}$$

Here η and η' are the viscosities of the lower and upper fluid. A few remarks on (31) are worth making:

- The dispersion relation ω_k is in general rather complicated. The simplification (32) derives from the approximation $\rho\omega_k \ll \eta k^2$ which is very well fulfilled for colloidal interfaces with extremely low surface tension. The approximation is controlled by the number

$$\frac{\xi}{L_\eta} = \left(\frac{\gamma^3 \Delta\rho}{g}\right)^{1/2} \frac{1}{(\eta+\eta')^2}, \tag{34}$$

  which is the ratio of the capillary length ξ to the viscous length $L_\eta = (\eta + \eta')^2/\gamma\Delta\rho$. It is very small, 10^{-5}, for colloidal interfaces, while it is very large for e.g. water (10^5).

- The spectrum has a slowest mode with wavelength ξ and decay rate t_c, in contrast to the capillary waves of molecular fluids, where the modes become slower the longer the wavelength. This mode starts to dominate the behavior of the correlations for long times.

6 The Langevin Equation

The thermal influences can be incorporated by a fluctuating force $F_{\mathbf{k}}(t)$ on mode $\mathbf{k}$ in the Langevin equation [15]

$$\frac{\partial h_{\mathbf{k}}}{\partial t} = -\omega_k h_{\mathbf{k}} + F_{\mathbf{k}}(t). \tag{35}$$

The first term on the right hand side is the systematic damping force, which by itself would lead to an exponential decay of mode k. The random force $F_{\mathbf{k}}(t)$ has zero average and is assumed to be δ–correlated in time (white noise)

$$\langle F_{\mathbf{k}}(t)\, F_{\mathbf{k}'}(t')\rangle = \delta_{\mathbf{k}+\mathbf{k}',\mathbf{0}}\, \Gamma_{\mathbf{k}}\, \delta(t-t'), \tag{36}$$

where $\Gamma_{\mathbf{k}}$ can be found from the fluctuation-dissipation theorem

$$\frac{\Gamma_{\mathbf{k}}}{2\omega_k} = \langle |h_{\mathbf{k}}|^2\rangle. \tag{37}$$

The Langevin equation (35) assumes that the slow capillary waves form a complete set to characterize the motion of the interface. $\Gamma_{\mathbf{k}}$ is linked in (37) to the equilibrium average of the amplitudes $h_{\mathbf{k}}$, which is given by (5).

With the Langevin equation all time-dependent correlation functions can be calculated. In particular the height-height correlation function follows as

$$\langle h(\mathbf{0},0)h(\mathbf{x},t)\rangle = \langle h^2\rangle g(x,t) = \sum_{\mathbf{k}} \langle |h_{\mathbf{k}}|^2\rangle \exp(i\mathbf{k}\cdot\mathbf{x} - \omega_k t), \tag{38}$$

with $\langle |h_{\mathbf{k}}|^2\rangle$ given by (6) and $\langle h^2\rangle$ by (8). Note that for this correlation function the influence of the fluctuating force $F_{\mathbf{k}}(t)$ averages out such that it is depends only on the macroscopic dynamics of the interface. It involves, apart from the decay rate ω_k only the thermal average $\langle |h_{\mathbf{k}}|^2\rangle$. Some properties of the integral yielding this function are listed in the Appendix.

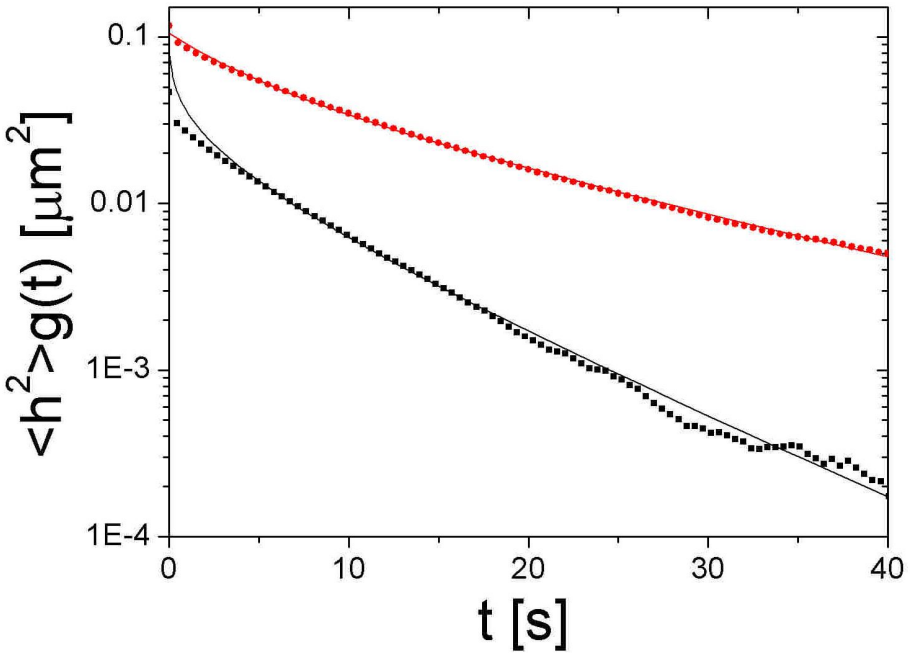

Figure 6: The correlation function $\langle h(0,t)h(0,0)\rangle$. The points are experimental values and the lines curves according to (40) using a cut-off.

The first point is the determination of γ and t_c from the data. We represent $\langle h(\mathbf{0},0)h(\mathbf{0},t)\rangle$ as

$$\langle h(\mathbf{0},0)h(\mathbf{0},t)\rangle = \frac{k_BT}{2\pi\gamma}H(t/t_c,\kappa), \tag{39}$$

Here again $\kappa = k_{max}\xi$. In the Appendix we prove that

$$H(t/t_c,\infty) = K_0(t/t_c), \tag{40}$$

with K_0 the modified Besselfunction of order 0. For $t \geq t_c/\kappa$, the function $H(t/t_c,\kappa)$ is well represented by $K_0(t/t_c)$. Since κ is of the order 40 to 50 (see Section 2), expression (40) suffices for most of the measured points, except of course for the first few points near $t = 0$, where the right hand side of (40) diverges. Leaving them out for the moment, we find from a fit for statepoint II: $t_c = 20s$ and $\gamma = 66nN/m$ and for statepoint IV: $t_c = 33s$ and $\gamma = 22nN/m$. Effectively t_c acts as a horizontal scale parameter and γ as a vertical shift. t_c is mainly determined by the asymptotic behavior, while γ is more sensitive to the initial behavior.

By adjusting the upper cut-off, the calculated $g(0,t)$ assumes the value 1 for $t = 0$. In Fig. 6 we plot the experimental values of $\langle h^2\rangle g(0,t)$ together with the theoretically calculated curves.

Finally we mention the initial behavior of $g(0,t)$. From the expansion (62) we deduce

$$g(0,t) = 1 - \frac{t}{t_c}\frac{\kappa}{\ln(1+\kappa^2)} + \cdots \tag{41}$$

Here one sees that a finite κ is essential for this initial behavior.

7 Probabilities on Histories

The noise term comes into the picture when we calculate the distribution of the $h_{\mathbf{k}}(t)$. It follows from the Fokker-Planck equation, which is equivalent with the Langevin

equation and reads [15]

$$\frac{\partial P(h_{\mathbf{k}},t)}{\partial t} = \omega_k \frac{\partial h_{\mathbf{k}} P(h_{\mathbf{k}},t)}{\partial h_{\mathbf{k}}} + \frac{\Gamma_{\mathbf{k}}}{2} \frac{\partial^2 P(h_{\mathbf{k}},t)}{\partial h_{\mathbf{k}}^2}. \tag{42}$$

It gives the evolution of the probability distribution $P(h_{\mathbf{k}},t)$ starting from an initial distribution $P(h_{\mathbf{k}},0)$. The solution [15] of (42) provides the conditional probability of the mode $h_{\mathbf{k}}(t)$, starting with the value $h_{\mathbf{k}}(0)$

$$P(h_{\mathbf{k}}(0)|h_{\mathbf{k}}(t)) = \frac{1}{[2\pi\langle|h_{\mathbf{k}}|^2\rangle(1-e^{-2\omega_k t})]^{1/2}} \exp -\frac{|h_{\mathbf{k}}(t) - h_{\mathbf{k}}(0)e^{-\omega_k t}|^2}{2\langle|h_{\mathbf{k}}|^2\rangle(1-e^{-2\omega_k t})}. \tag{43}$$

The expression shows that, independent of the value of $h_{\mathbf{k}}(0)$, the distribution asymptotically approaches the equilibrium distribution (5).

For the measurements at different times (and possibly different positions) we need the multiple time correlation function

$$G_n(h_1,\mathbf{x}_1,t_1;\cdots;h_n,\mathbf{x}_n,t_n) = \langle\delta(h(\mathbf{x}_1,t_1)-h_1)\cdots\delta(h(\mathbf{x}_n,t_1)-h_n)\rangle, \tag{44}$$

giving the probability of a *history* that the interface is at time t_1 and position $\mathbf{x}_1$ at a height h_1 and subsequently at time t_i and position $\mathbf{x}_i$ at height h_i. In order to evaluate these correlation functions we have to translate the field $h(\mathbf{x},t)$ into its fourier components $h_{\mathbf{k}}$. Then we have to use the joint probability on a set of components $h_{\mathbf{k}}(t_1),\cdots h_{\mathbf{k}}(t_n)$, which is given by the product of the equilibrium probability (8) for the first event at t_1 and the conditional probabilities (43) for the successive time intervals, $t_2-t_1,\cdots,t_n-t_{n-1}$. The result of the integration can be derived easily from the observation that the $h(\mathbf{x}_j,t_j)$ are, as linear combinations of the basic variables $h_{\mathbf{k}}$, also gaussian random variables. So, similar to the derivation of (12), their distribution must be of the form

$$G_n(h_1,\cdots,t_n) = \left(\frac{\det g^{-1}}{(2\pi\langle h^2\rangle)^n}\right)^{1/2} \exp\left[-\frac{1}{2}\sum_{i,j} g^{-1}_{i,j}\frac{h_i h_j}{\langle h^2\rangle}\right]. \tag{45}$$

The matrix $g_{i,j}$ is the correlation matrix

$$g_{i,j} = g(|\mathbf{x}_i - \mathbf{x}_j|, t_i - t_j) \tag{46}$$

The proof of (45) is exactly the same as that of (12).

(45) is the main result of the theory for the histories. It relates the probability of a history $h_1,\cdots,h_n$ on a sequence of snapshots to the height-height correlation function $g(x,t)$. The strong point of (45) is that the time-dependent probability densities have exactly the same structure as the equal time probabilities, when expressed in the appropriate $g_{i,j}$. Thus the whole analysis given above for the equal time correlations, can be taken over for the more general correlations. So we restrict ourselves for the time dependent histories to the aspects needing some extra attention.

The time dependent probability density G_2 reads as (20) with $g = g(0,t)$. It can also be written as the product of the equilibrium distribution $P_{eq}(h_1)$ and the conditional probability $G_c(h_1,0,0|h_2,0,t)$ that starting at h_1 one arrives at h_2 at time t later

$$G_c(h_1,0,0|h_2,0,t) = \frac{1}{[2\pi(1-g^2)]^{1/2}} \exp -\frac{[h_2 - h_1 g]^2}{2[1-g^2]}. \quad (47)$$

This expression cannot be seen as the "propagator" for the probability, like (43) is for the fourier components $h_{\mathbf{k}}$. While the probabilities for the modes $\mathbf{k}$ evolve as a Markov process, the distribution for $h(\mathbf{0},t)$ does have a memory effect. Only if $g(0,t)$ were a pure exponential the spatial process would be Markovian too [15]. The expression (38) shows that $g(0,t)$ it is not a pure exponential but a superposition of exponentials. For longer times it starts to decay as an exponential when the slowest mode begins to dominate, as can be seen in Fig. 6.

8 Average numbers of hills and valleys

Consider now a sequence of snapshots, taken with time intervals Δt. We are again interested in the probabilities on the duration of "hills" and "valleys" with respect to a level h. To stress the analogy between space and time we use the same notation $p_n^{\pm}(h)$ for the probabilities to find a stretch of exactly n consecutive values of the interface height above/level the level h, where n now is an index in the time direction. They are given by the same integrals as (22) and (23) with $g_{i,j}$ the temporal correlation matrix. The mean values are called the *residence time* $\tau^+(h)$ (for $p_n^+(h)$) and the *waiting time* $\tau^-(h)$ (for $p_n^-(h)$).

To check whether the experimental values follow these theoretical predictions, we first checked that the ratio $\tau^+(h)/\tau^-(h)$ is the same $q^+(h)/q^-(h)$ in analogy with 27. It is valid over several orders of magnitude. Only for the very large h deviations occur due to poor statistics. In Fig. 7 we now plot again the calculated values of $q^{+-}(h,g)$ as function of the parameter $g = g(0,t)$, for a number of h values. The upper curve in Fig. 7 for $h = 0$, is given by equation (29). In this figure the experimental values are plotted as follows. We take as time interval a multiple n of the smallest interval Δt and determine for this sampling rate the τ's. This leads to experimental values of $q^{+-}(h,g)$, which we plot in the figure at the value $g = g(n\Delta t)$. The curves for a fixed value of h are statepoint independent; the figure shows that this is pretty well the case.

Finally we plot in Figure 8 the dependence of the τ's on h for three choices of the time interval. The curves are confusing at first sight, since the values of $\tau^{\pm}(h)$ are about the same for all three choices. So, if we multiply them with the value of the chosen time interval, in order to convert them from numbers to real times, we get substantial different times. This indicates that the residence and waiting time depend strongly on the measuring process.

The fact that the smallest chosen time interval leads to the smallest value of the residence and waiting time, naturally poses the question what will happen in the limit of vanishingly small time interval Δt. Theoretically it relies on the behavior of the correlation function $g(t)$ in the limit $t \to 0$. We presented in (41) the behavior as it follows from capillary wave theory. A linear approach of g to 1 implies that $\tau^{+-}(h)$ increases as the inverse power of the square root of Δt. Then, after multiplying with

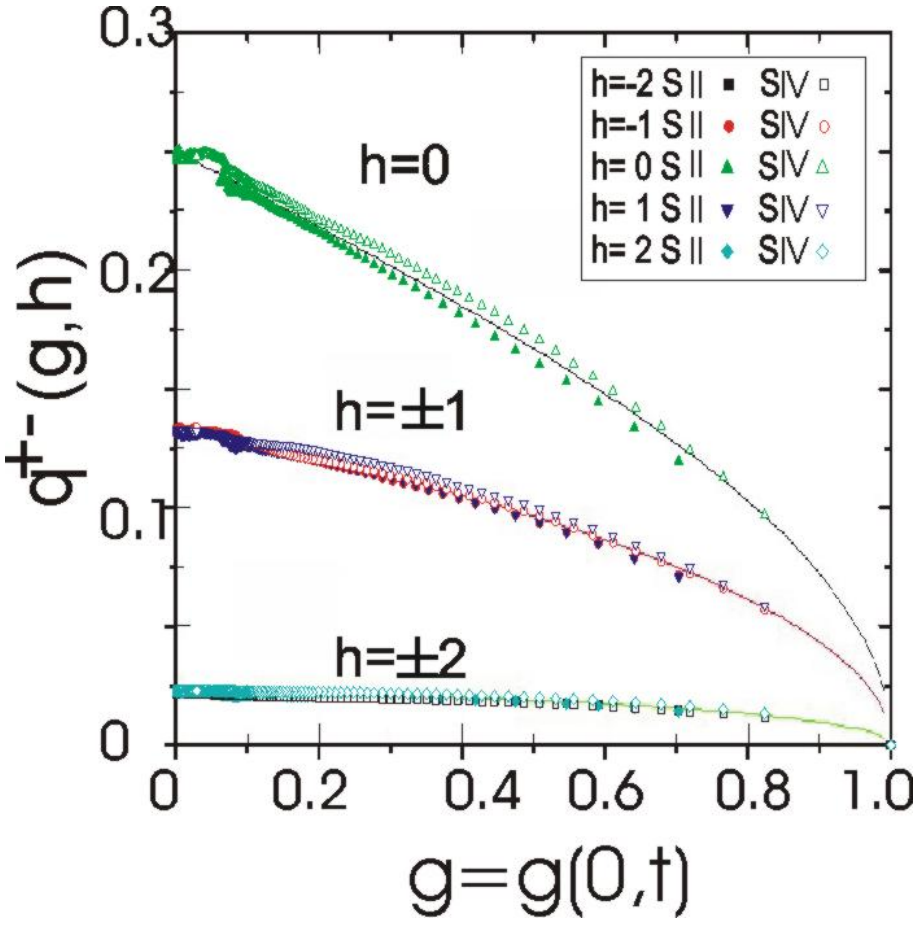

Figure 7: The function q^{+-} as function of t represented by $g = g(0,t)$, for $h = -1$ (filled squares), $h = 0$ (circles) and $h = 1$ (semifilled pentagons). The colours correspond to time intervals $\Delta t = 0.5$ seconds (black symbols), $2\Delta t$ (red symbols) and $4\Delta t$ (green symbols). The drawn lines are calculated and the points are the measured values.

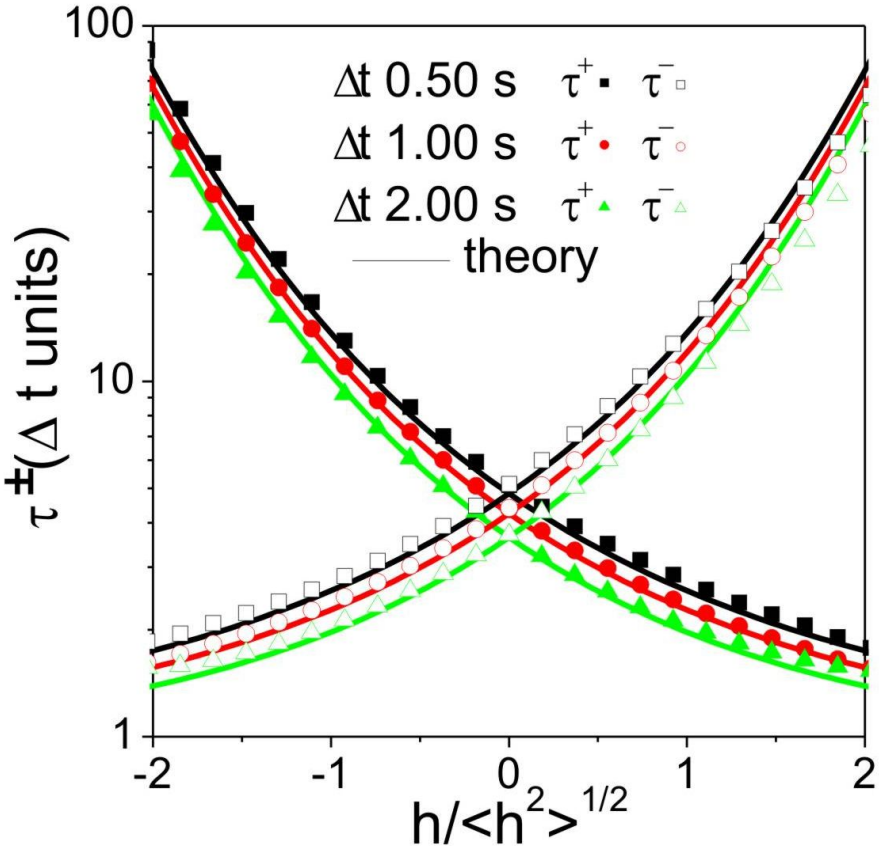

Figure 8: values of $\tau^{\pm}(h)$ as function of h for three time interval for three interval $\Delta t, 2\Delta t$ and $4\Delta t$.

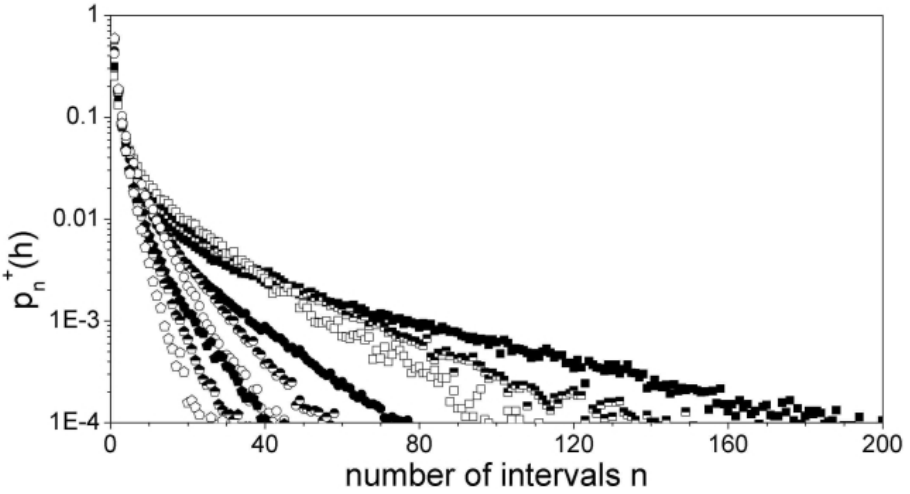

Figure 9: The temporal $p_n^+(h)$ for statepoint IV, for $h = -1$ (filled squares), $h = 0$ (circles) and $h = 1$ (semifilled pentagons). The colours correspond to time intervals $\Delta t = 0.5$ seconds (black symbols), $2\Delta t$ (red symbols) and $4\Delta t$ (green symbols)

Δt in order to get their values in real time, the residence and waiting time vanish as the square root of Δt. However, the slope of the linear term in (41) depends on a molecular quantity κ, which indicates that wavelengths matter for which the mesoscopic capillary waves theory is not designed [5]. One could argue that for molecular times, the cusp in $g(0,t)$ is rounded off to a parabola (since it is time reversal invariant). Then this parabola would compensate the square root in (30) and the residence and waiting time would approach a finite limit.

Unfortunately this scenario can not be tested experimentally, given the present limits on the sampling frequency. However, there is an interesting sampling regime beyond our data, for which the capillary wave theory still holds. In Fig. 7 the data go up to the value $g \simeq 0.8$. The typical square root decay of the curves for $q^{+-}(h,g)$ cannot be tested with our data. A microscope, which is faster by a factor 10, could enter this regime where the typical signature of the Brownian character of the fluctuations is most significant. They give increasingly larger weight to short living hills and valleys, which force the mean values to shrink in a specific way predicted by the presented theory.

The same issue presents itself in the analysis of the data for a single time as function of the sampling distance, but in a less severe way. In the appendix it is shown that the height-height correlation as function of the distance is a parabola for short distances. Thus a finite value of the sequence length and the recurrence length would follow in the limit of continuous sampling. However, again we do not reach the regime and the theoretical limiting values are strongly dependent on the cut-off κ, where the capillary wave theory breaks down.

9 Dependence of $p_n^{\pm}(h)$ on n and h

We plot in Fig. 9 the experimental curves for $p_n^+(h)$ for a large number of n for statepoint IV. A noteworthy point is that only for rather large values of n the decay with n (time) becomes exponential. The scatter in the data is modest, even for large n corresponding to large times t. Thus the experiment provides a host of detailed

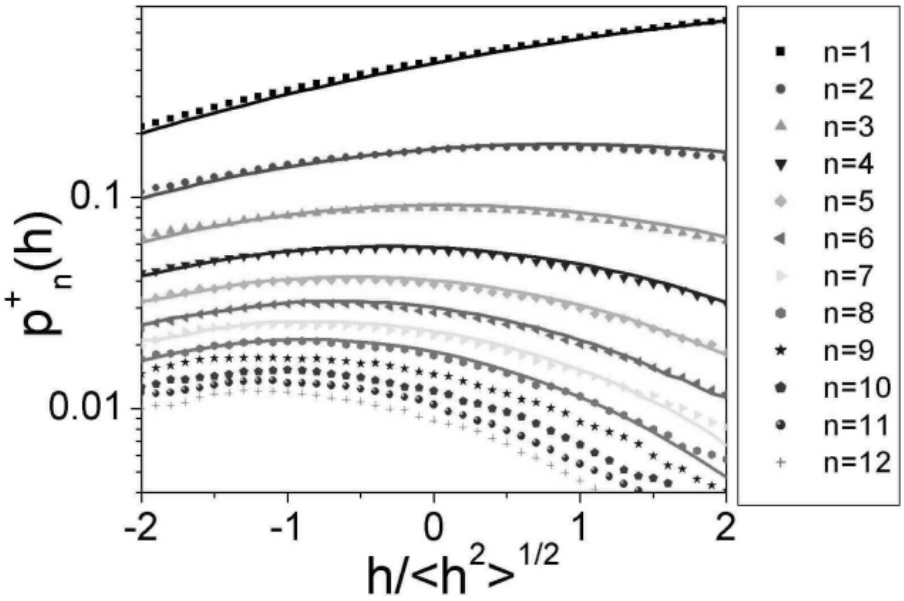

Figure 10: The temporal $p_n^+(h)$ as function of h for a number of n for statepoint IV. The drawn lines are the theoretical values.

information on the statistics of the fluctuations in a wide time range.

Another way of plotting the data is to select one value of n and plot $p_n^{\pm}(h)$ as function of h. Fig. 10 shows the experimental data for statepoint IV for $p_n^+(h)$. This way of presenting the data facilitates the comparison with the theory. The drawn lines are the theoretical values as given by (21). We reiterate that the input in the calculations is a set of $n+2$ experimental values of $g(0,t)$. The agreement between theory and experiment is remarkable for these detailed data. Statepoint II gives similar results with a slight asymmetry between up and down, of the same type as deviations in the spatial correlation functions, shown in Fig. 5.

The data for $p_n^-(h)$ have been independently collected. The symmetry (25) is very well obeyed, such that there is no point in showing these data separately.

10 Discussion

The above given analysis of the statistics of interface fluctuations naturally falls into two parts, in which the height-height correlation function $g(x,t)$ plays a pivotal role. The first part concerns the connection between $g(x,t)$ and the state parameters such as $\Delta\rho, \eta$ and γ. The second part is the determination of the multiple correlation-functions $G(h_1, \cdots, t_n)$ from $g(x,t)$ through (45). In the first part we have used the data for $g(x,t)$ to determine the state parameters. Even though the derivation of the structure of $g(x,t)$ in space and in time is quite different, the behavior is remarkably similar if the space and time variables are properly scaled (see (10) and (40)).

The second part has been our main concern. We used the measured $g(x,t)$ as input, providing all the necessary information on the statistics of the snapshots. The advantage of splitting the problem into these two parts is that the second part is not confounded by errors in the first. The only assumption in the theory is the use of the Langevin equation for the effect of the thermal (white) noise. The best justification for this procedure is *a posteriori* through its consequences. In view of the successful agreement with the experimental results, the assumption appears to be very well

fulfilled.

Experimentally the capillary waves are disentangled from the structure of the intrinsic interface. Most amazing is that detailed correlations in capillary waves can be determined with high accuracy. The statistics of the temporal dependence is generally better than that of the spatial behavior. We have chosen only a limited set of obtainable correlation functions in order to compare them with the theoretical calculations. Experimentally it is easy to collect data for practically any interesting n. In Fig. 5 and Fig. 9 we show the distribution $p_n^+(h)$ as function of n for the values $h = -1, 0$ and 1.

There is a simplifying aspect in the fact that experimentally only sequences of finite time intervals can be measured. So one does not know what the interface does in between two snapshots. But this is precisely the reason why it suffices to calculate the correlation functions defined in Section 4. Here also one does not specify the evolution in between two snapshots. For instance, the key quantity $q^{+-}(h, g)$ for the residence and waiting times, involves the crossing of the level h by the interface. But it does not say that it may cross it only once! Any odd number of crossings is possible. In Fig. 7, where we compare $q^{+-}(h, g)$ with experiment, large time intervals feature (corresponding to small g) and in these large time intervals crossings are frequently taking place. Also the hills and valleys of length n for which the distribution is given in Fig. 5 and Fig. 10, may be interrupted by opposite values in between snapshots. The charm of the comparison is that both theory and experiment allow these possibilities.

In this paper we have restricted ourselves to sequences of height measurements at the same time or at the same position. The general result (45) shows that one could equally well correlate snapshots at combinations of times and positions and do a similar statistical analysis. The only point that matters is the height-height correlation $g_{i,j}$ between the events i and j. Also one does not need to worry in how much the measurements refer to a single point or to an area of finite size. These more collective variables are also linear combinations of the basic variables $h_{\mathbf{k}}$ and therefore also gaussian randomly distributed. Then taking the measured correlations between the more general variables as input, leads to exactly the same analysis as given here for point variables.

Acknowledgments The authors are indebted for valuable discussions with D.G.A.L. Aarts, H.W.J. Blöte, G.T. Barkema and members of the "Theorieclub", where this problem arose. We also thank J. de Folter, C. Vonk, S. Sacanna and B. Kuipers for help with the synthesis and characterisation of the experimental system. The work of VWAdV is part of the research program of the 'Stichting voor Fundamenteel Onderzoek der Materie (FOM)', which is financially supported by the 'Nederlandse Organisatie voor Wetenschappelijk Onderzoek (NWO)'. Support of VWAdV by the DFG through the SFB TR6 is acknowledged.

A The height-height correlation integral

In this appendix we discuss some properties of the height-height correlation function $g(x, t)$. We start with the equal time function $g(x, 0)$. Using the scaled integration variable $y = k\xi$ the integral for $g(x, 0)$ leads to

$$g(x,0) = \frac{2}{\log(1+\kappa^2)} \int_0^\kappa y dy \frac{J_0(xy/\xi)}{1+y^2} \tag{48}$$

where $\kappa = k_{max}\xi$ is the cut-off. Sending this value to ∞ yields the modified Bessel-function K_0

$$\int_0^\infty ydy \frac{J_0(xy/\xi)}{1+y^2} = K_0(x/\xi) \tag{49}$$

For finite κ we can make a short distance expansion, reading

$$\int_0^\kappa ydy \frac{J_0(xy/\xi)}{1+y^2} = \frac{1}{2}\log(1+\kappa^2) + \left(\frac{x}{\xi}\right)^2 \left(\frac{\kappa^2 - \log(1+\kappa^2)}{2}\right) + \cdots \tag{50}$$

Matching the small argument expansion of $K_0(x/\xi)$

$$K_0(x/\xi) = \log(x/2\xi) - 0.57721 + \cdots \tag{51}$$

with (50) gives for the point where they cross the approximate value

$$x \simeq \frac{\xi}{\kappa} \tag{52}$$

The behavior in the time direction is remarkably similar to the spatial direction, although the integral for $g(0,t)$ looks quite different. We write

$$g(0,t) = \frac{2}{\log(1+\kappa^2)} H(t/t_c;\kappa), \tag{53}$$

with $H(z;\kappa)$ as the integral

$$H(z;\kappa) = \int_0^\kappa \frac{ydy}{1+y^2} \exp[-z(y+y^{-1})/2]. \tag{54}$$

The first point is to prove relation (40), which we do by showing that

$$\frac{dH(z,\infty)}{dz} = -K_1(z). \tag{55}$$

and checking the asymptotic expansion of (40) for large z. The advantage of (55) is that

$$\frac{dH(z;\infty)}{dz} = -\frac{1}{2}\int_0^\infty dy \exp[-z(y+y^{-1})/2] \tag{56}$$

is a simpler integral than (54). Then take $x = \ln y$ as integration variable, which turns (56) into

$$\frac{dH(z;\infty)}{dz} = -\frac{1}{2}\int_{-\infty}^\infty dx\, e^x \exp(-z\cosh x). \tag{57}$$

Splitting the integral into pieces from $-\infty$ to 0 and from 0 to ∞ and changing in the first part from x to $-x$, yields the relation

$$\frac{dH(z;\infty)}{dz} = -\int_0^\infty dx \cosh x \exp(-z\cosh x). \tag{58}$$

The integral is a representation of the function $K_1(z)$ [16].

In order to show that no constant is lost in going from (40) to (55) one can check the asymptotic expansion of (40) for large z, which follows from an expansion around the slowest mode for $y = 1$:

$$y + y^{-1} = 2 + (y-1)^2 + \cdots \tag{59}$$

and replacing the integral by a full gaussian around $y = 1$. Then one gets

$$H(z;\infty) \simeq \frac{e^{-z}}{2} \int_{-\infty}^{\infty} d(y-1) \exp[-(y-1)^2 z/2] = e^{-z} \left(\frac{\pi}{2z}\right)^{1/2}, \quad (60)$$

which matches the asymptotic expansion of $K_0(z)$.

The final point is the expansion for small times t/t_c for a finite value of κ. We expand the exponential

$$\exp[-(y+y^{-1})z/2] = 1 - (y+y^{-1})z/2 + \cdots \quad (61)$$

and insert this expansion into the integral (54). Then we find for $H(z;\kappa)$

$$H(z;\kappa) = \frac{1}{2}\ln(1+\kappa^2) - \frac{\kappa}{2}\, z + \cdots \quad (62)$$

Note that the next term in this expansion leads to a logarithmically divergent integral at the small y side. Thus the next term is not of the order z^2 but of the order $z^2 \ln z$. The finite κ integral stays finite in contrast to $K_0(z)$ which diverges for $z = 0$. With the expansion (51) and (62) we find for the point where the finite-κ curve starts to deviate from the $K_0(z)$:

$$t \simeq t_c/\kappa. \quad (63)$$

One obtains the rough estimate $z \simeq 1/\kappa$ for this matching point, by looking to the value of the exponential at the upper boundary, which is $\exp[-z(\kappa + \kappa^{-1})/2]$. For larger values the boundary value starts to vanish and extending the integral to infinity leads to a small error. For smaller values of this z, the exponent of the exponential becomes smaller than 1 at the boundary and the integrand of (54) has not yet died out at $y = \kappa$. Then deviations from the infinite domain start to show up.

References

[1] J.D. van der Waals, Z. Phys. Chem. **13** (1894) 657.

[2] M.V. von Smoluchowski, Ann. Phys. **25** (1908) 205.

[3] L. Mandelstam, Ann. Phys. **41** (1913) 609-624.

[4] F.P. Buff, R.A. Lovett and F.H. Stillinger, Phys. Rev. Lett. **15** (1965) 621.

[5] J.D. Weeks, J. Chem. Phys. **67** (1977) 3106.

[6] C.V. Raman, Nature, 112 (1923) 281.

[7] A. Vrij, Adv. Coll. Interf. Sci. **2** (1968) 36-64

[8] A. Braslau, P.S. Pershan, G. Swislow, B.M. Ocko and J. Als-Nielsen, Phys Rev A **38** 2457 (1988).
M.K. Sanyal, S.K. Sinha, K,G. Huang and B.M. Ocko, Phys. Rev. Lett. **66** (1991) 628.
C. Fradin, A Braslau, D. Luzet, D. Smilgies. M. Alba, N. Boudet, K. Mecke and J. Daillant, Nature, **403** (2000) 871.

[9] J.H. Sikkenk, J.M.J. van Leeuwen, E.O. Vossnack and A.F. Bakker, Physica **146A** (1987) 622-633.

[10] D.G.A.L. Aarts, M. Schmidt and H.N.W. Lekkerkerker, Science **304** (2004) 847; D. Derks, D. Aarts, D. Bonn, H.N.W. Lekkerkerker, and A. Imhof, Phys. Rev. Lett. **97** 038301 (2006); D.G.A.L. Aarts and H.N.W. Lekkerkerker, J. Fluid Mech., **606** 275-294 (2008).

[11] B. Vincent. Colloids Surf., **50** (1990) 241.

[12] H.N.W. Lekkerkerker, W.C.K. Poon, P.N. Pusey, A. Stroobants and P.B. Warren, Phase behaviour of colloid + polymer mixtures. Europhys. Lett. **20** (1992) 559.

[13] V.W.A. de Villeneuve, J.M.J. van Leeuwen, J.W.J. de Folter, D.G.A.L. Aarts, W. van Saarloos and H.N.W. Lekkerkerker, Europhys. Lett., **81**, 60004 (2008).

[14] U-Ser Jeng, L. Esibov, L. Crow and A Steyerl, J. of Condens. Matter **16S** (1998) 4231.

[15] N.G. van Kampen, *Stochastic Processes in Physics and Chemistry*, Elsevier, 3rd edition, 2007.

[16] M. Abramowitz and I.E. Stegun, *Handbook of Mathematical Functions*, Dover, 9th edition, 1972.